Queensland University of Technology
Brisbane Australia

This is the author's version of a work that was submitted/accepted for publication in the following source:

Smith, Ryan N., Chyba, Monique, & Singh, Shashi B. (2008) Decoupled trajectory planning for a submerged rigid body subject to dissipative and potential forces. In *IEEE Region 10 Colloquium and Third International Conference on Industrial and Information Systems*, 8-10 December 2008, Kharagpur, India.

This file was downloaded from: http://eprints.qut.edu.au/40140/

© Copyright 2008 Please consult the authors.

Notice: *Changes introduced as a result of publishing processes such as copy-editing and formatting may not be reflected in this document. For a definitive version of this work, please refer to the published source:*

Decoupled Trajectory Planning for a Submerged Rigid Body Subject to Dissipative and Potential Forces

Monique Chyba
Department of Mathematics
University of Hawaii
Honolulu, HI 96822
Email: mchyba@math.hawaii.edu

Ryan N. Smith
Ocean & Resources Engineering
University of Hawaii
Honolulu, HI 96822
Telephone: (808) 956–9244
Fax: (808) 956–9139
Email: ryan@math.hawaii.edu

Shashi B. Singh
Department of Mathematics
University of Hawaii
Honolulu, HI 96822
Email: sbsingh@math.hawaii.edu

***Abstract*—This paper studies the practical but challenging problem of motion planning for a deeply submerged rigid body. Here, we formulate the dynamic equations of motion of a submerged rigid body under the architecture of differential geometric mechanics and include external dissipative and potential forces. The mechanical system is represented as a forced affine-connection control system on the configuration space $\mathrm{SE}(3)$. Solutions to the motion planning problem are computed by concatenating and reparameterizing the integral curves of decoupling vector fields. We provide an extension to this inverse kinematic method to compensate for external potential forces caused by buoyancy and gravity. We present a mission scenario and implement the theoretically computed control strategy onto a test-bed autonomous underwater vehicle. This scenario emphasizes the use of this motion planning technique in the under-actuated situation; the vehicle loses direct control on one or more degrees of freedom. We include experimental results to illustrate our technique and validate our method.**

Keywords: Autonomous Underwater Vehicles, Geometric Control, Kinematic Reduction, Under-actuated.

I. Introduction

Recently, there has been a growing interest in the scientific community to impart greater autonomy to underwater vehicles to perform a multitude of tasks in the complex oceanic environment. In contrast to the motion planning problem for terrestrial vehicles, an Autonomous Underwater Vehicle (AUV) can exploit six degrees of freedom (DOF) for movement and is subjected to many more external forces acting upon the body. Such an environment further motivates research into the trajectory and control strategy design for underwater vehicles.

With the growing volume of sea trade, underwater vehicles may be employed to carry out regular inspections of ship hulls and in some cases even perform repairs. Such applications not only reduce expenses, but also eliminate the need for human involvement. Whether it be inspection, observation or intervention, successful completion of any application requires careful planning to generate controlled trajectories which steer these vehicles to their desired goals.

To this end, we provide some solutions to the motion planning problem through the implementation of geometric control theory. Designing the control strategies in this manner allows us to exploit symmetries and inherent nonlinearities in the dynamic structure of these mechanical systems. This paper is motivated by the desire to apply mathematical rigor to solve challenging motion planning problems for a submerged rigid body and implement these theories onto a test-bed AUV. This is an effort to bridge the gap between thoeretical calculations and practical applications related to the motion planning problem for underwater vehicles.

We present a theoretical model for a submerged rigid body built with the tools of differential geometry. These equations of motion are presented as a second order system and include dissipative drag forces and those potential forces arising from gravity and buoyancy. The motion planning problem is solved via inverse kinematics and decoupled trajectory planning using a kinematic reduction. Previous publications (e.g. [1], [2]) have shown that the dissipative drag forces can be accounted for in the kinematic reduction, however the potential forces have not yet been included in the extension of this theory. In this paper, we propose an *ad-hoc* method of including the potential forces over the duration of a given trajectory.

In the following section, we present a short derivation of the equations of motion of a rigid body submerged in a real (viscous) fluid. In Section III, we develop the theory necessary to attack the motion planning problem using a kinematic reduction and present results of recent works. Section IV is devoted in computing the control strategy to be implemented onto a test-bed AUV. Finally, in Section V we present the experimental results obtained from the implementation of the computed control strategy.

II. Equations of Motion

The general equations of motion for a rigid body submerged in a viscous fluid have many representations, (see for example

[3] or [4]). Here we present these equations under the architecture of differential geometry. For a detailed motivation of the advantages of expressing the equations in this manner, we refer the reader to [4] and [5]. In the case of the submerged rigid body, the configuration space is given by the manifold $Q = \mathbb{R}^3 \times \mathrm{SO}(3) = \mathrm{SE}(3)$.

For a neutrally-buoyant submerged rigid body with the center of gravity (C_G) and center of buoyancy (C_B) coincident, the dynamic equations of motion are given by an affine-connection control system on Q by

$$\widetilde{\nabla}_{\gamma'}\gamma' = \sum_{a=1}^{6} \sigma^a(t)\mathbb{I}_a^{-1}(\gamma(t)), \tag{1}$$

where $\widetilde{\nabla}$ represents a modified Levi-Civita connection with the property that

$$\widetilde{\nabla}_{X_i}X_j = \begin{cases} -\frac{D_i}{\mathbb{G}_{ii}}X_i & i = j \\ \nabla_{X_i}X_j & i \neq j \end{cases}, \tag{2}$$

for X_i a standard basis vector for $\mathrm{SE}(3)$. Details on the modification of the Levi-Civita affine connection can be found in [1] and [2]. Additionally, $\mathbb{I}_i^{-1} = \mathbb{G}^{\#}\pi_i = \mathbb{G}^{ij}X_j$, which may be represented as the i^{th} column of the inertia matrix $\mathbb{I}^{-1} = \begin{pmatrix} M^{-1} & 0 \\ 0 & J^{-1} \end{pmatrix}$, and $\sigma_i(t)$ are the controls. The M and J are 3×3 matrices which account for the mass and added mass of the vehicle. These matrices are assumed diagonal since our test-bed vehicle has three planes of symmetry and we choose the origin of the body-fixed reference frame to be located at C_G. We define $D_i = C_{D_i}\rho A_i$ where $i \in \{1, ..., 6\}$ denotes the respective degree of freedom in which the velocity is applied.

In practice, it is unlikely that an AUV will have $C_G = C_B$ due to stability concerns. Also, for safety reasons, submersibles are generally constructed to be slightly positively buoyant. To account for these induced potential forces, we must extend the previously presented equations of motion. First, we denote by $r_{C_G} = (x_G, y_G, z_G)$ ($r_{C_B} = (x_B, y_B, z_B)$) the location of C_G (C_B) with respect to the origin of the body fixed frame. We define a rotation matrix $R \in \mathrm{SO}(3)$ which describes the orientation of the body with respect to the earth fixed reference frame. Also, let r_B denote the vector from the center of the earth fixed reference frame to C_B. Now, the potential force from the acceleration due to gravity acts directly at C_G, and is given by the potential function $V_G(\gamma(t)) = W(Rr_B + b) \cdot k$ where $W = mg$ is the weight of the rigid body, $\cdot$ denotes the inner product and k is a unit vector pointing in the direction of gravity. Similarly, the force arising from the buoyancy is the force exerted by the fluid on the submerged volume of the vessel and acts at C_B and is given by the potential function $V_B(\gamma(t)) = B(Rr_B + b) \cdot k$, where $B = \rho g \mathcal{V}$ and ρ is the fluid density, g is the acceleration due to gravity and $\mathcal{V}$ is the submerged volume of the body. These two potential forces can be combined into one term denoted by $P(\gamma(t)) = -(dV_G + dV_B)$. Writing this in matrix form we can express the potential forces from gravity and buoyancy as geometric accelerations with the following:

$$G^{\#}P(\gamma(t)) = \begin{bmatrix} \frac{1}{m_1}(W-B)s\theta \\ -\frac{1}{m_2}(W-B)c\theta s\phi \\ -\frac{1}{m_3}(W-B)c\theta c\phi \\ -\frac{1}{j_1}((y_G W - y_B B)c\theta c\phi + (z_G W - z_B B)c\theta s\phi) \\ \frac{1}{j_2}((z_G W - z_B B)s\theta + (x_G W - x_B B)c\theta c\phi) \\ -\frac{1}{j_3}((x_G W - x_B B)c\theta s\phi - (y_G W - y_B B)s\theta) \end{bmatrix}, \tag{3}$$

where s and c represent sin and cos respectively. The musical exponent $^{\#}$ implies a tangent bundle isomorphism which literally means *divide by mass*, turning the force into an acceleration. Note that if $C_G \neq C_B$, the two opposing potential forces will induce a torque, referred to as the righting moment, if the vehicle rotates. The righting arm GZ depends on the distance between C_G and C_B and the list angle ϕ as seen in Figure 1. On the other hand, if $C_G = C_B$, then the vehicle will experience no torque that opposes orientational displacements. Combining this derivation with (1), we have the following theorem for the general equations of motion.

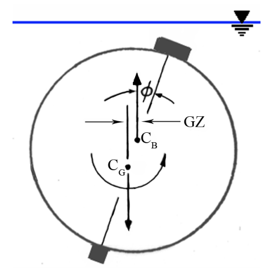

Figure 1. Potential forces acting at C_G and C_B and the righting arm for a submerged spherical vehicle.

THEOREM **II.1.** *The equations of motion of a rigid body submerged in a viscous fluid and subjected to dissipative and potential forces are given by the forced affine-connection control system:*

$$\widetilde{\nabla}_{\gamma'}\gamma' = -G^{\#}P(\gamma(t)) + \sum_{i=1}^{6}\mathbb{I}_i^{-1}(\gamma(t))\sigma_i(t). \tag{4}$$

III. CONTROL STRATEGY

The method used for the control strategy design will follow the decoupled motion planning method presented first in [6] and expanded upon in [4]. However, in these references, the controls are computed for a neutrally buoyant vehicle submerged in an ideal fluid such that $C_G = C_B$. In [2], this method was extended to include dissipative hydrodynamic drag experienced in a viscous fluid through the modification of the affine connection. In this paper, we push the extension slightly further and show a preliminary method to include potential forces for this type of control design.

The decoupled motion planning method used here applies a kinematic reduction to the second order affine connection control system. This reduction yields a first order system on Q for which kinematic motions can be planned using decoupling

Table I
COVARIANT DERIVATIVES IN BASIS NOTATION FOR THE CONNECTION $\widetilde{\nabla}$. HERE $(i,j) = \nabla_{\mathbb{I}_i^{-1}} \mathbb{I}_j^{-1}$.

$(1,1)$	$\frac{D_1}{m_1} X_1$	$(2,1)$	$-\frac{1}{2}\frac{(m_1-m_2)}{j_3} X_6$
$(1,2)$	$-\frac{1}{2}\frac{(m_1-m_2)}{j_3} X_6$	$(2,2)$	$\frac{D_2}{m_2} X_2$
$(1,3)$	$-\frac{1}{2}\frac{(m_3-m_1)}{j_2} X_5$	$(2,3)$	$\frac{1}{2}\frac{(m_3-m_2)}{j_1} X_4$
$(1,4)$	0	$(2,4)$	$-\frac{1}{2}\frac{(m_3-m_2)}{m_3} X_3$
$(1,5)$	$\frac{1}{2}\frac{(m_3-m_1)}{m_3} X_3$	$(2,5)$	0
$(1,6)$	$\frac{1}{2}\frac{(m_1-m_2)}{m_2} X_2$	$(2,6)$	$\frac{1}{2}\frac{(m_1-m_2)}{m_1} X_1$
$(3,1)$	$-\frac{1}{2}\frac{(m_3-m_1)}{j_2} X_5$	$(4,1)$	0
$(3,2)$	$\frac{1}{2}\frac{(m_3-m_2)}{j_1} X_4$	$(4,2)$	$\frac{1}{2}\frac{(m_3+m_2)}{m_3} X_3$
$(3,3)$	$\frac{D_3}{m_3} X_3$	$(4,3)$	$-\frac{1}{2}\frac{(m_3+m_2)}{m_2} X_2$
$(3,4)$	$-\frac{1}{2}\frac{(m_3-m_2)}{m_2} X_2$	$(4,4)$	$\frac{D_4}{j_1} X_4$
$(3,5)$	$\frac{1}{2}\frac{(m_3-m_1)}{m_1} X_1$	$(4,5)$	$\frac{1}{2}\frac{(j_3+j_2-j_1)}{j_3} X_6$
$(3,6)$	0	$(4,6)$	$-\frac{1}{2}\frac{(j_3+j_2-j_1)}{j_2} X_5$
$(5,1)$	$-\frac{1}{2}\frac{(m_3+m_1)}{m_3} X_3$	$(6,1)$	$\frac{1}{2}\frac{(m_2+m_1)}{m_2} X_2$
$(5,2)$	0	$(6,2)$	$-\frac{1}{2}\frac{(m_2+m_1)}{m_1} X_1$
$(5,3)$	$\frac{1}{2}\frac{(m_3+m_1)}{m_1} X_1$	$(6,3)$	0
$(5,4)$	$-\frac{1}{2}\frac{(j_3-j_2+j_1)}{j_3} X_6$	$(6,4)$	$-\frac{1}{2}\frac{(j_3-j_2-j_1)}{j_2} X_5$
$(5,5)$	$\frac{D_5}{j_2} X_5$	$(6,5)$	$\frac{1}{2}\frac{(j_3-j_2-j_1)}{j_1} X_4$
$(5,6)$	$\frac{1}{2}\frac{(j_3-j_2+j_1)}{j_1} X_4$	$(6,6)$	$\frac{D_6}{j_3} X_6$

vector fields. These kinematic motions are guaranteed to be solutions to the dynamic (second order) system, and the dynamic controls can be computed. For details please see [4]. One reason for the consideration of this motion planning strategy is that it easily allows the consideration of a vehicle operating in an under-actuated (distressed) condition.

The aforementioned decoupling vector fields are kinematic reductions of rank one. The integral curves of these vector fields define the admissible motions for kinematic control inputs. We call these integral curves the kinematic motions. By concatenating these kinematic motions, we can compute solutions to the motion planning problem.

A necessary and sufficient condition for a vector field V to be decoupling for an affine connection control system is that V and $\nabla_V V$ are sections of the input distribution of vector fields. Thus, decoupling vector fields are calculated by considering the covariant derivatives of the input vector fields to the system. For the affine connection $\widetilde{\nabla}$, the covariant derivatives of the input vector fields in basis notation corresponding to motion in a real fluid are displayed in table I. Before we present the control strategy developed from this strategy, we must first discuss the test-bed AUV and its specific hydrodynamic parameters.

A. Test-bed Vehicle

The test-bed AUV we use is the Omni-Directional Intelligent Navigator (ODIN) which is owned and operated by the Autonomous Systems Laboratory (ASL), College of Engineering at the University of Hawaii. The experiments conducted for this research are carried out at the Duke Kahanamoku Swimming Complex at the University of Hawaii.

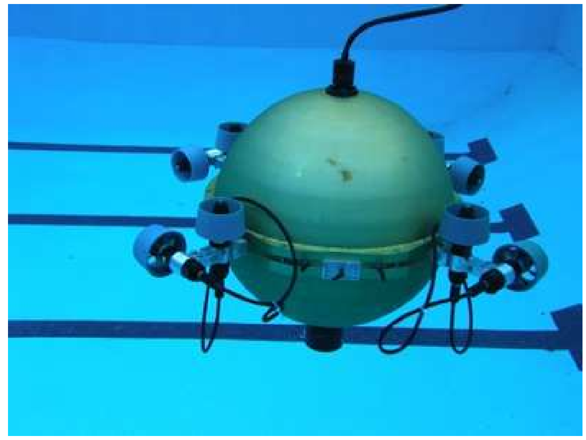

Figure 2. ODIN operating in the pool.

As seen in Figure 2, ODIN has a spherical hull which is 65cm in diameter. This sphere is constructed from an aluminum alloy to prevent corrosion. Eight thrusters are attached to the sphere via four fabricated mounts, each holding two thrusters. The thrusters are evenly distributed around the sphere with four vertical and four horizontal. Fully assembled, ODIN weighs $126.55kg$ and is positively buoyant by $\approx 2N$. More details on ODIN, including numerical values of the various hydrodynamic parameters can be found in [7].

Unique to ODIN's construction is the control from an eight dimensional thrust to move in six DOF. This construction puts redundancy into the system in case of thruster failure. It is important to distinguish between a control for the real vehicle, namely the applied control referring to the action of the thrusters, and the six DOF control referring to the principle axes in the body fixed frame. Our input trajectories to ODIN take the form of the six DOF controls which are converted on-board ODIN to the control for the eight actual thrusters using the following Thrust Control Matrices (TCM's).

$$TCM_{hor} = \begin{bmatrix} -0.707 & 0.707 & 0.707 & -0.707 \\ 0.707 & 0.707 & -0.707 & -0.707 \\ 0.48160 & -0.48160 & 0.48160 & -0.48160 \end{bmatrix} \quad (5)$$

$$TCM_{ver} = \begin{bmatrix} -1.0 & -1.0 & -1.0 & -1.0 \\ -0.26989 & -0.26989 & 0.26989 & 0.26989 \\ 0.26989 & -0.26989 & -0.26989 & 0.26989 \end{bmatrix} \quad (6)$$

These transformations are based on the assumption that we can decouple the action of the thrusters since the distance between C_G and C_B is small relative to the diameter of the vehicle. The horizontal thrusters contribute only to motion in surge, sway and yaw, while the vertical thrusters contribute only to motion in heave, roll and pitch.

B. Motion Planning

With the above information, we are now ready to consider the motion planning problem and compute the dynamic controls for a given trajectory. In the fully-actuated scenario, we can achieve any final configuration through the concatenation of at most six pure motions. Thus, without any obstacles, the motion planning problem is uninteresting. To this end, we consider an under-actuated scenario for our test-bed AUV. By under-actuated, as following with the development of the equations of motion, the vehicle is unable to apply direct control in one or more of the six DOF. With ODIN, there are two under-actuated situations which arise naturally and deserve first consideration. First is the loss of the horizontal thruster set T_H. This leaves us only able to directly control heave, roll and pitch. Similarly, the other scenario is the loss of vertical thruster set T_V which leaves us only having direct control on surge, sway and yaw. Since the under-actuation definition corresponds to the loss of degrees of freedom and not directly to the loss of an individual thruster or thrusters, these two scenarios are the most favorable to consider. Research is ongoing to compute the decoupling vector fields for an affine-connection control system with eight input vector fields such that each input directly corresponds to one of ODIN's thrusters.

Since the purpose of this paper is to provide a first extension of decoupled trajectory planning using kinematic motions to compensate for potential forces, we consider the under-actuated situation where ODIN can only utilize the vertically oriented thrusters and prescribe a final configuration which requires the vehicle to maintain an angular displacement so as to invoke righting moments to counteract. In this situation, we have three input vector fields, $\{\mathbb{I}_3^{-1}, \mathbb{I}_4^{-1}, \mathbb{I}_5^{-1}\}$ for the dynamic system. The equations of motion given in (4) then reduce to

$$\widetilde{\nabla}_{\gamma'}\gamma' = -G^{\#}P(\gamma(t)) + \sum_{i=3}^{5} \mathbb{I}_i^{-1}(\gamma(t))\sigma_i(t). \qquad (7)$$

Using only the vertical thrusters, ODIN is kinematically controllable meaning that she can realize any configuration through a concatenation of kinematic motions, see [8] for a proof of this fact. Given the input controls in the under-actuated situation, it is interesting to prescribe a final configuration such that the vehicle realizes a pure surge motion. If we begin at the origin, we would like to end at $\eta_{final} = (a, 0, 0, 0, 0, 0)$. Since we have direct control on heave, realizing $\eta_1 = (a, 0, b, 0, 0, 0)$ would solve the motion planning problem since we could then simply apply a pure heave to reach η_{final}, or let the buoyancy force slowly take ODIN upwards. For our example in this paper, we will take $\eta_{final} = (1.25, 0, 2.5, 0, 0, 0)$, where the distances are given in meters.

IV. Control Strategy Design

As mentioned previously, the control design is computed using inverse kinematics from the trajectory created via the concatenation of kinematic motions. Given that the input control vector fields are $\mathcal{I}_3^{-1} = \{\mathbb{I}_3^{-1}, \mathbb{I}_4^{-1}, \mathbb{I}_5^{-1}\}$, a simple calculation shows that the decoupling vector fields for this system are the constant multiples and linear combinations of the set $\mathcal{V} = \{X_3 = (0, 0, 1, 0, 0, 0), X_4 = (0, 0, 0, 1, 0, 0), X_5 = (0, 0, 0, 0, 1, 0)\}$.

To realize this motion, the basic idea is to point the bottom of ODIN at η_{final} by following the integral curves of $-X_4$ (pitch motion), then follow the integral curves of X_3 (heave motion) to realize the displacement. At the end of the body-pure heave motion, the vehicle will be in the configuration $(1.25, 0, 2.5, 0, -25.3°, 0)$. We can then undo the pitch motion by following the integral curves of X_4.

Assuming that $C_G = C_B$ the above plan will provide the appropriate trajectory for the vehicle. However, for ODIN $C_G \neq C_B$ and we encounter righting moments which need to be compensated. However, these induced forces remain constant throughout the body-pure heave motion.

The discussed motion planning techniques using a kinematic reduction only work on *driftless* systems. In particular, the use of a kinematic reduction is only effective on systems in which the input controls are the only external forces. As seen in (4), the term $\mathbb{G}^{\#}P(\gamma(t))$ gives our considered system a drift. Hence, known techniques will not work to develop dynamic controls to steer the vehicle between two given configurations. Through experimentation with the test-bed vehicle, we have developed an *ad-hoc* method of including the potential forces. This method is what we will present in the control strategy design and implementation.

As a first method for compensation of the induced potential forces and moments, we neglect the geometric theory for the rotations at the beginning and end of the trajectory. Instead, we apply the appropriate controls to compensate for the forces and moments induced by a pitch angle of $-25.3°$ for a period of 5s in order to allow the vehicle to stabalize. While still applying this control we additionally apply the appropriate controls to realize a 2.92m body-pure heave. At this point, we have reached $(1.25, 0, 2.5, 0, -25.3°, 0)$ and now need only to undo the angular displacement. To do this we simply turn off all controls and allow the vehicle to right itself.

We continue by computing the controls required to achieve the previously discussed motion. First, we use (3) along with the fact that $(W - B) = -2$ to compute

$$P(\gamma(t)) = \begin{bmatrix} 0.85 \\ 0 \\ -1.81 \\ 0 \\ -3.71 \\ 0 \end{bmatrix}, \qquad (8)$$

which gives the six dimensional forces which need to be compensated in order to maintain a pitch angle of $-25.3°$.

To calculate the controls for the body-pure heave, we revert back to the geometric method utilizing the decoupling vector fields. A detailed description of the inverse kinematics used can be found in [4] and is omitted here due to space limitations.

We wish to follow the integral curves of the decoupling vector field X_3. The dynamic controls can then be computed using Theorem 13.5 in [4] which simplifies to the following equation

$$\sigma^3(t)\mathbb{I}_3^{-1}(\gamma\circ\tau(t)) = (\tau\,'(t))^2\nabla_{X_3}X_3(\gamma\circ\tau(t)) + \tau\,''(t)X_3(\gamma\circ\tau(t)), \tag{9}$$

where $\tau(t)$ is a reparameterization of the curve $\gamma(t)$ such that the vehicle will begin and end the motion with zero velocity. For this motion, we choose $\tau(t) : [0,8] \mapsto [0,2.92]$ such that $\tau(t) = \frac{73t^2(12-t)}{6400}$. The covariant derivative in the above equation can be computed using the results displayed in Table I. Given the velocity of this motion and the hydrodynamic parameters of ODIN, we use $m_3 = 196$ and $D_3 = 115$.

Direct computation shows that the dynamic control strategy steering ODIN from $\eta_{init} = (0,0,0,0,0,0)$ to $\eta_{final} = (1.25,0,2.5,0,0,0)$ is given by $\sigma(t) = (-0.85,0,1.81,0,3.71,0)$ for $t\in[0,5]$ followed by

$$\sigma(t) = \begin{cases} -0.85 \\ 0 \\ 115\tau\,'(t)^2 + 196\tau\,''(t) + 1.81 \quad t\in[5,13]. \\ 0 \\ 3.71 \\ 0 \end{cases} \tag{10}$$

We then set every control to zero at $t = 13$ to finalize the motion. This theoretical strategy is a continuously evolving thrust strategy with respect to time, which requires a few more steps before implementation. Since our end goal is to implement such strategies onto ODIN, we must take the physical thrusters into account. Two main features to note are a finite limit on the thrust which can be output by each thruster and the incapability of instantaneous switches from one direction to another. Also, a continuously evolving control strategy requires too much onboard data storage to be practical. These limitations force us to construct strategies which are piece-wise constant with the pieces connected via linear junctions occurring over a short time interval. For ODIN, we use a 0.9 second time interval to switch the controls.

Changing the continuous control structure to a piece-wise constant control structure yields the following implementable control strategy. For the body-pure heave motion, the piece-wise constant control sturcture is computed by ensuring that the integral of the control strategy as a function of time, the work done, is the same as that given by the continuous control strategy.

Notice here that we include an induced force in the surge component. In the under-accuated situation we consider, we can not compensate for this force. The actual applied control strategy is the same as that given in Table II with the surge control set to zero throughout. In the next section we present the implementation results of the under-accuated scenario as well as the fully-actuated situation for comparison.

Table II
PIECE-WISE CONSTANT CONTROL STRUCTURE FOR TRAJECTORY ENDING AT $\eta_{final} = (1.25,0,2.5,0,0,0)$ COMPENSATING FOR POTENTIAL FORCES.

Time (s)	Applied Thrust (6-dim)
0	(0,0,0,0,0,0)
0.9	(-0.85,0,1.81,0,3.71,0)
5.9	(-0.85,0,1.81,0,3.71,0)
6.8	(-0.85,0,25.71,0,3.71,0)
12.513	(-0.85,0,25.71,0,3.71,0)
13.413	(-0.85,0,-16.75,0,3.71,0)
15.7	(-0.85,0,-16.75,0,3.71,0)
16.6	(0,0,0,0,0,0)

V. EXPERIMENTS

In this section we implement the control strategies developed from the theory in the previous sections. As mentioned previously, the test-bed AUV is ODIN and the experiments are carried out in the diving well at the Duke Kahanamoku Aquatic Complex at the University of Hawaii. In order to simulate a fully submerged vehicle for the implementation, each mission begins with a closed-loop pure heave to 1m and stabilization in all angular orientations. This location is considered $\eta_{init} = (0,0,0,0,0,0)$. Since the depth sensor reads 1m at the initial configuration, for the experiments we understand that $\eta_{final} = (1.25,0,3.5,0,0,0)$. The computed control strategies are then implemented from the initial configuration in a fully open-loop manner. Since we are interested in the ability to design trajectories using kinematic motions, we do not impose any feedback controls.

We first present the experimental results obtained from the implementation of the under-actuated control strategy shown in Fig. 3. Considering the evolution of the surge and heave, we see that experimental results match very well with theoretical predictions. The vehicle realizes a surge displacement just greater than the prescribed 1.25m and the final depth is roughly 3.5m as predicted. We see some deviation in sway which is attributed to non-zero yaw and roll evolutions. Since we are implementing the strategies in open-loop, we are unable to correct for any parasite thrusts which arise.

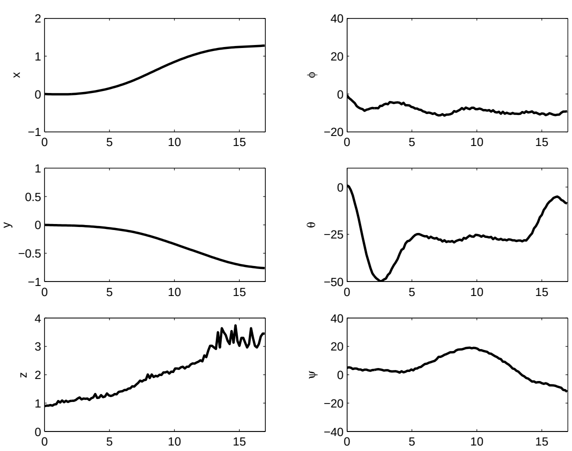

Figure 3. Experimental evolutions of the AUV in under-actuated condition for $\eta_{final} = (1.25,0,3.5,0,0,0)$

If we now consider the evolution of pitch for the duration of the trajectory, we see that after an initial overshoot of the prescribed angle, the vehicle was able to maintain a rather consistent pitch throughout the entire body-pure heave. We also make note that the $-25°$ pitch was maintained after the five seconds of given stabilization time. This time was determined through many experimental trials.

It is important to note that the final configuration was essentially realized even when we neglected to account for the induced force in the surge component. Referring back to (8), we see that the induced force in surge was 0.85N. Since the under-actuated condition did not allow ODIN to account for this force, the vehicle overshot the proposed target for surge. To demonstrate that neglecting this surge force does not significantly alter the results, we present the experimental results of the implementation of the fully actuated scenario in Fig. 4.

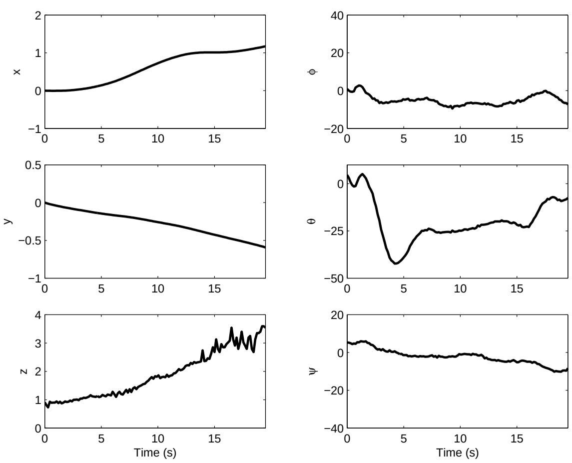

Figure 4. Experimental evolutions of the AUV in fully-actuated condition for $\eta_{final} = (1.25, 0, 3.5, 0, 0, 0)$

We note here that the results displayed in the two figures are very similar. The slight difference to take note of is that in Fig. 4, the surge evolution precisely reaches 1.25m as prescribed. This difference is due to the compensation being made for the induced surge force.

VI. Conclusion

In this paper, we have seen the successful implementation of control strategies designed using geometric reduction techniques. As mentioned in Section V, the experimental results corresponded well with theoretical predictions. This presentation validates the chosen *ad-hoc* method to include the potential forces within our control design procedure.

We note here that under normal operating conditions, an AUV will generally not be required to maintain a constant list angle in pitch or roll. Thus, potential forces arising from a separation of C_B and C_G upon listing would only need compensation if the trajectory requires an angular displacement to realize a final configuration. This scenario is most prevalent in an under-actuated condition where the vehicle for one reason or another has lost direct control on one or more degrees of freedom. As seen in our presentation, we were able to realize a pure surge motion without direct control of the surge force component.

The under-actuated condition considered here demonstrates the usefulness of the method of inclusion of the potential forces. However, this simple scenario is far from generating the control structure for a solution to the general motion planning problem for a submerged rigid body. The next phase, which is currently under study, is to incorporate these potential forces in a more rigorous theoretical formulation rather than the *ad-hoc* method presented in this paper. It is of interest to note that the interplay between theory and application has permitted the extension of kinematic motion planning with excellent results. Taking what we learn from the experimental results will help further the development of the theory and hopefully lead to better implementations and more complex trajectory and control designs.

References

[1] M. Chyba, R. N. Smith, G. Wilkens, and C. Catone, "A geometrical approach to the motion planning problem for a submerged rigid body," March 2008, submitted for publication to the International Journal of Control.

[2] M. Chyba and R. N. Smith, "A first extension of geometric control theory to underwater vehicles," in *Proceedings of the 2008 IFAC Workshop on Navigation, Guidance and Control of Underwater Vehicles*, Killaloe, Ireland, 2008.

[3] T. I. Fossen, *Guidance and Control of Ocean Vehicles*. John Wiley & Sons, 1994.

[4] F. Bullo and A. D. Lewis, *Geometric Control of Mechanical Systems*. Springer, 2005.

[5] A. D. Lewis, "Is it worth learning differential geometric methods for modelling and control of mechanical systems?" 2007, unpublished.

[6] F. Bullo and K. Lynch, "Kinematic controllability for decoupled trajectory planning in underactuated mechanical systems," *IEEE Transactions. Robotics and Automation*, vol. 17, no. 4, pp. 402–412, 2001.

[7] M. Chyba, T. Haberkorn, R. N. Smith, and S. Choi, "Design and implementation of time efficient trajectories for an underwater vehicle," *Ocean Engineering*, vol. 35, no. 1, pp. 63–76, 2008.

[8] M. Chyba, T. Haberkorn, R. Smith, and G. Wilkens, "A geometrical analysis of trajectory design for underwater vehicles," *Discrete and Continuous Dynamical Systems-B*, 2008, accepted, to be published.